Artificial Intelligence Study

Three-Dimensional Lumbosacral Reconstruction by An Artificial Intelligence-Based Automated MR Image Segmentation for Selecting the Approach of Percutaneous Endoscopic Lumbar Discectomy

Zhaoyin Zhu, PhD[1#], Enqing Liu, MD[1#], Zhihai Su, PhD[2#], Weijian Chen, PhD[3], Zheng Liu, PhD[4], Tao Chen, PhD[2], Hai Lu, PhD[2], Jin Zhou, PhD[1*], Qingchu Li, MD[1*], and Shumao Pang, PhD[5*]

From: [1]Southern Medical University, Guangzhou, Guangdong, China; [2]The Fifth Affiliated Hospital of Sun Yat-sen University, Spine Surgery, Zhuhai, Guangdong, China; [3]The Fifth Affiliated Hospital of Guangzhou Medical University, Guangzhou, Guangdong, China; [4]Southern University of Science and Technology Hospital, Shenzhen, Guangdong, China; [5]School of Biomedical Engineering, Guangzhou Medical University, Guangzhou, Guangzhou, Guangdong, China

Address Correspondence: Shumao Pang, PhD School of Biomedical Engineering, Guangzhou Medical University, Guangzhou, Guangzhou, Guangdong, China E-mail: pangshumao@126.com

Disclaimer: Z Zhu, E Liu, and Z Su contributed equally to this work and share first authorship. J Zhou, Q Li, and S Pang contributed equally to this work and share last authorship. See pg E253 for funding information.

Conflict of interest: Each author certifies that he or she, or a member of his or her immediate family, has no commercial association (i.e., consultancies, stock ownership, equity interest, patent/licensing arrangements, etc.) that might pose a conflict of interest in connection with the submitted manuscript.

Manuscript received: 08-06-2023
Revised manuscript received: 10-07-2023
Accepted for publication: 10-11-2023

Free full manuscript: www.painphysicianjournal.com

Background: Assessing the 3-dimensional (3D) relationship between critical anatomical structures and the surgical channel can help select percutaneous endoscopic lumbar discectomy (PELD) approaches, especially at the L5/S1 level. However, previous evaluation methods for PELD were mainly assessed using 2-dimensional (2D) medical images, making the understanding of the 3D relationship of lumbosacral structures difficult. Artificial intelligence based on automated magnetic resonance (MR) image segmentation has the benefit of 3D reconstruction of medical images.

Objectives: We developed and validated an artificial intelligence-based MR image segmentation method for constructing a 3D model of lumbosacral structures for selecting the appropriate approach of percutaneous endoscopic lumbar discectomy at the L5/S1 level.

Study Design: Three-dimensional reconstruction study using artificial intelligence based on MR image segmentation.

Setting: Spine and radiology center of a university hospital.

Methods: Fifty MR data samples were used to develop an artificial intelligence algorithm for automatic segmentation. Manual segmentation and labeling of vertebrae bone (L5 and S1 vertebrae bone), disc, lumbosacral nerve, iliac bone, and skin at the L5/S1 level by 3 experts were used as ground truth. Five-fold cross-validation was performed, and quantitative segmentation metrics were used to evaluate the performance of artificial intelligence based on the MR image segmentation method. The comparison analysis of quantitative measurements between the artificial intelligence-derived 3D (AI-3D) models and the ground truth-derived 3D (GT-3D) models was used to validate the feasibility of 3D lumbosacral structures reconstruction and preoperative assessment of PELD approaches.

Results: Artificial intelligence-based automated MR image segmentation achieved high mean Dice Scores of 0.921, 0.924, 0.885, 0.808, 0.886, and 0.816 for L5 vertebrae bone, S1 vertebrae bone, disc, lumbosacral nerves, iliac bone, and skin, respectively. There were no significant differences between AI-3D and GT-3D models in quantitative measurements. Comparative analysis of quantitative measures showed a high correlation and consistency.

Limitations: Our method did not involve vessel segmentation in automated MR image segmentation. Our study's sample size was small, and the findings need to be validated in a prospective study with a large sample size.

Conclusion: We developed an artificial intelligence-based automated MR image segmentation method, which effectively segmented lumbosacral structures (e.g., L5 vertebrae bone, S1 vertebrae bone, disc, lumbosacral nerve, iliac bone, and skin) simultaneously on MR images, and could be used to construct a 3D model of lumbosacral structures for choosing an appropriate approach of PELD at the L5/S1 level.

Key words: 3D lumbosacral reconstruction, artificial intelligence, automated magnetic resonance image segmentation, percutaneous endoscopic lumbar discectomy, preoperative assessment

Pain Physician 2024: 27:E245-E254

The percutaneous endoscopic lumbar discectomy (PELD) procedure, which has 2 main approaches, namely the transforaminal approach (TF-PELD) and the interlaminar approach (IL-PELD), has become increasingly popular as minimally invasive spinal surgery (1-3). According to one recent meta-analysis, lumbar disc herniation (LDH) might be better treated with IL-PELD than TF-PELD owing to shorter operation time and fewer fluoroscopies (4). TF-PELD, however, seems to be a better choice for LDH patients, as it results in less blood loss and a shorter incision, according to another meta-analysis (5). At the L5/S1 level, PELD approaches are primarily determined by the surgeon's preferences and clinical experience since neither approach has strong evidence in support (4,5). Nevertheless, due to the anatomical complexity of the TF-PELD approach for L5/S1 LDH, even experienced surgeons might require longer operation time to overcome bone structure barriers (6,7). If the greater possibility of bony structure obstruction and lumbosacral nerve injury is pre-assessed for L5/S1 TF-PELD, IL-PELD or open lumbar microdiscectomy is considered a better surgical option. Furthermore, a complete understanding of the detailed soft tissues, such as the dura mater, nerve, and skin, remains reasonably necessary for avoiding nerve root injury and dural tears for planning optimal surgical trajectory for the L5/S1 TF-PELD (8,9). Therefore, assessing the relationship between critical anatomical structures and surgical channels would help select PELD approaches at the L5/S1 level.

Preoperative evaluation methods using medical images have been widely used in research and clinical settings (10,11) to determine the possibility of bony structure obstruction and subsequently plan an optimal surgical trajectory for L5/S1 TF-PELD. The existing preoperative evaluation methods mainly rely on 2-dimensional (2D) medical images by x-ray (11) and Computed tomography (CT) fluoroscopy (10). Nevertheless, the single plane of 2D medical images is incapable of directly and quickly identifying an accessible trajectory, and sometimes, the single plane shows no accessible pathway on all axial slices (12). Instead, 3-dimensional (3D) lumbosacral reconstruction may benefit the viability assessment of the L5/S1 TF-PELD. Recent studies have used CT images to predict surgical difficulty for the L5/S1 TF-PELD using 3D lumbosacral reconstruction (13). 3D lumbosacral reconstruction is effective in predicting the viability of TF-PELD. However, CT fluoroscopy possesses radiation properties, and 3D lumbosacral reconstruction's accuracy could be affected by poor soft tissue contrast. MR images, with superior soft-tissue contrast, offer benefits for the 3D lumbosacral reconstruction accuracy over x-ray and CT images. Despite this, no study has investigated whether 3D lumbosacral reconstruction would increase the effectiveness of L5/S1 TF-PELD selection on MR images.

Artificial intelligence has recently been widely adopted to segment targeted structures on medical images (14-16). Some studies of automated magnetic resonance image segmentation and 3D reconstructions for spinal structures with artificial intelligence have been published (17-19). Previous studies have neglected the automatic segmentation and 3D reconstruction of the iliac bone and skin (19,20), but the 3D reconstruction of these structures is crucial for the preoperative evaluation of the L5/S1 TF-PELD. Thus, our study aimed to assess:

1. Whether artificial intelligence was effective in simultaneously achieving automated multi-class MR image segmentation of spinal structures (vertebrae bone, disc, lumbosacral nerves, iliac bone, and skin).
2. Whether 3D lumbosacral reconstruction of automated multi-class MR image segmentation was effective and reliable.
3. Whether 3D lumbosacral reconstruction of MR images would benefit the L5/S1 TF-PELD selection.

Methods

Participant Characteristics

Informed consent forms were signed by all participants before the start of the study, which was approved by the Ethics Committee of our hospital (2020 K05-1). 3D T2-weighted sampling perfection with application-optimized contrast with various flip-angle evolutions (3D T2W-SPACE) sequences (21) scans were performed for all participants at the L5/S1 level using a 3T MR unit (Magnetom Verio; Siemens, Erlangen, Germany). Participants had to meet the following inclusion criteria: (1) over 18 years of age and (2) no contraindications to undergo MR imaging. We excluded participants with previous spinal surgery, congenital abnormalities, lumbar spondylolisthesis, instability, malformation, other severe mental and physical diseases, active infection, and pregnancy. Fifty participants between March and July 2020 were finally included in the study. The age of participants ranged from 23 to 84 years (mean, 43.7 years). Patients' body mass index ranged from 17.72 to 33.03 kg/m^2 (mean, 24.00 kg/m^2).

Automatic Segmentation

Fifty MR data samples at the L5/S1 level were used to develop an artificial intelligence algorithm for automatic segmentation. Manual segmentation and labeling of vertebrae bone (L5 and S1 vertebrae bone), disc, lumbosacral nerve, iliac bone, and skin by 3 experts were used as the ground truth in Mimics 19.0 (Materialise, Leuven, Belgium) (Fig. 1A-1D). A lumbosacral structures segmentation was meticulously outlined by one expert, followed by an independent review by 2 more experts. Each expert voted on any areas that were disagreed upon. All MR datasets were preprocessed using resampling, cropping, and padding prior to training. An artificial intelligence algorithm, 3D U-net (22), was trained for automatic segmentation using Pytorch 1.5.1 (open-source, Facebook Artificial Intelligence Research). Fig. 1E shows a 3D U-net composed of an encoder (left path) and a decoder (right path). The input of the 3D U-net was an image of 128×128×128 image with a channel. Eight channels were present in the output: one for the background, one for the L5 vertebrae bone, one for the disc, one for the S1 vertebrae bone, one for the lumbosacral nerve, one for the iliac bone, and one for the skin. The size of convolutional kernels was 3×3×3 except for the last convolutional layer, which used a 1×1×1 convolutional kernel. Upsampling was achieved through trilinear interpolation. Five-fold cross-validation and quantitative metrics (including Dice score, precision, and recall) were used to evaluate the segmentation accuracy of artificial intelligence (14). Fifty MR data samples were divided into 5 groups randomly, with each group containing 10 samples serving as the test set; 40 samples (the other 4 groups) were divided into training and validation sets.

3D Lumbosacral Reconstruction

After the automatic segmentation, 3D masks of vertebrae bone (L5 and S1 vertebrae bone), discs, lumbosacral nerves, iliac bone, and skin were generated, which were then imported into Mimics 19.0 for 3D lumbosacral reconstruction. To validate the artificial intelligence-derived 3D (AI-3D) models (Fig. 2), we measured the shortest distance (Line A) between the crossing point (point a) of the superior and inferior articular process and the nerve root for all MR datasets with 3-matic 11.0 software (Fig. 3), and then compared it with that from the ground truth-derived 3D (GT-3D) models (Fig. 2A) under the same viewing angle in the 3D view mode. As the diameter of a commonly used working channel of TF-PELD was 8 mm, the crossing point of the superior and inferior articular process and the nerve root could be regarded as a key factor affecting the selection of the L5/S1 TF-PELD. Line A of AI-3D models and GT-3D models were measured independently by 2 experts. After a month, one of the independent experts remeasured Line A for each model.

TF-PELD Assessment

A cylindrical region (diameter = 8 mm, length = 150 mm, based on the size of a commonly used working channel of TF-PELD) was established as the virtual trajectory and was converted into the Standard Template Library (STL) data format. The STL, as the working channel of TF-PELD, was placed in the intervertebral foramen (IVF) to evaluate the difficulty degree of the L5/S1 TF-PELD with all 3D models. The detailed process is as follows: first, the target point (point b), as the center point of the proximal surgical trajectory, was defined as the cross-point of the medial line of the pedicle and the midline disc (Fig. 4A). Then, point c was defined as the cross-point of the lateral line of the surgical trajectory and iliac bone (Fig. 4B). Finally, STL was performed to place on each IVF of 3D models (Fig. 4B) according to the above 2 processes. If the STL-virtual trajectory did not touch these spinal structures, including the inferior articular process, transverse processes, and lumbosacral nerves, the IVF of the 3D model would be classified as Group A (Fig. 4C), for which selecting TF-PELD was advised; otherwise, these were classified as Group B, for which, selecting IL-PELD or open lumbar microdiscectomy was recommended.

To further validate the feasibility of TF-PELD assessment in Group A, the trajectory angle values in axial view and the entry point distance (Line B) measured from the median line to the tentative skin entry point (point d was defined as the cross-point of the midline trajectory and skin) between AI-3D models and GT-3D models were measured independently by two experts (Fig. 4D). After a month, an independent expert remeasured the trajectory abduction angle and the entry point distance.

Statistical Analysis

SPSS Statistics version 26.0 was used for all statistical analyses (IBM Corporation, Armonk, NY). A Wilcoxon signed-rank test and Pearson's correlation coefficient analysis were used to compare the associated differences in quantitative measurements between AI-3D models and GT-3D models without assuming an underlying distribution. $P < 0.05$ denoted statistical

significance. The intraobserver and interobserver reliabilities were assessed using the intraclass correlation coefficient (ICC) (23).

Results

Artificial intelligence-based automated MR image segmentation achieved high mean Dice scores of 0.921,

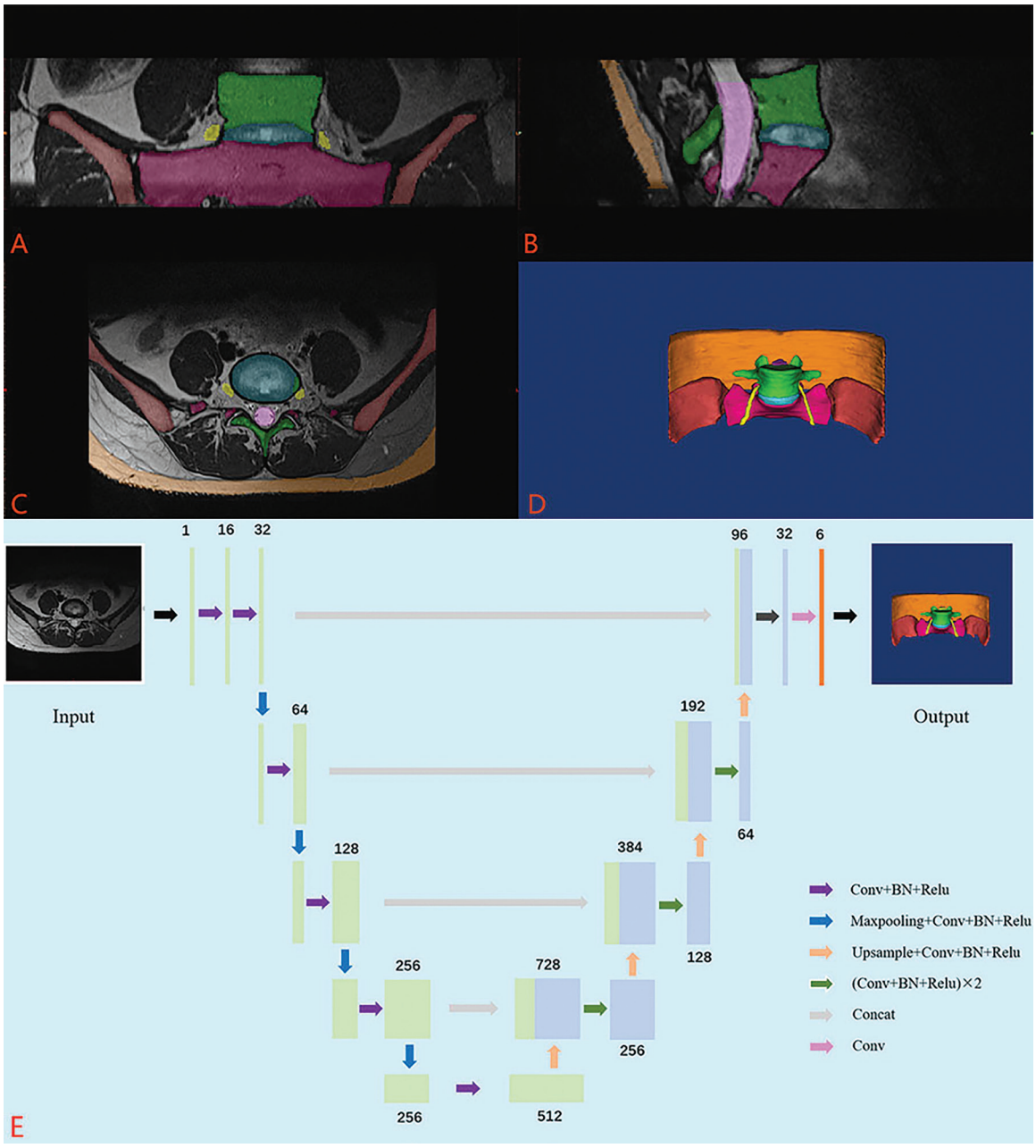

Fig. 1. *3D lumbosacral reconstruction based on magnetic resonance (MR) image segmentation. Manual MR image segmentations of targeted structures for building ground truth are shown in coronal (A), sagittal (B), transverse (B), and 3D views (B); schematic drawing of the 3D U-net based on automated MR image segmentation (E).*

0.924, 0.885, 0.808, 0.886, and 0.816 for L5 vertebrae bone, S1 vertebrae bone, disc, lumbosacral nerves, iliac bone, and skin, respectively (Fig. 5A). The mean precision of artificial intelligence for the L5 vertebrae bone, S1 vertebrae bone, disc, lumbosacral nerves, iliac bone, and skin were 0.939, 0.928, 0.879, 0.830, 0.897 and 0.821, respectively (Fig. 5B). The mean recall of artificial intelligence for the L5 vertebrae bone, S1 vertebrae bone, disc, lumbosacral nerves, iliac bone, and skin were 0.906, 0.923, 0.907, 0.800, 0.883 and 0.845, respectively (Fig. 5C). As shown in Table 1, a detailed quantitative evaluation of segmentation metrics was performed. The artificial intelligence-based automated MR image segmentation took 2.5 seconds per level, which was significantly less than manual segmentation (8.5 hours).

For the 3D lumbosacral reconstruction, there were no significant differences between AI-3D models and

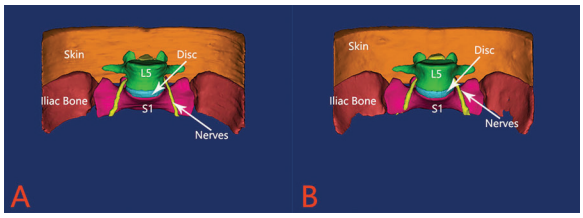

Fig. 2. *3D lumbosacral models were generated from manual segmentation A) and automatic segmentation, B) under the same viewing angle.*
L5: 5th lumbar vertebra; S1: 1st sacral vertebra.

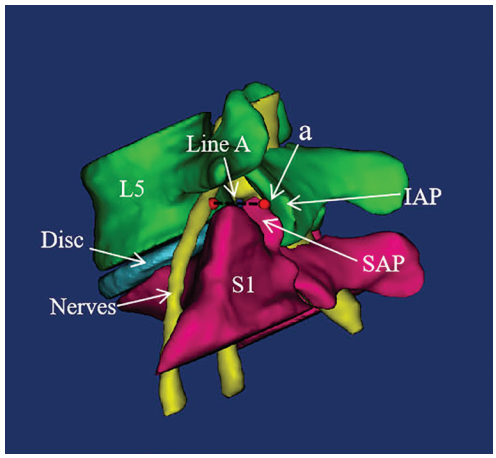

Fig. 3. *3D lumbosacral models were generated from manual segmentation. L5: 5th lumbar vertebra; S1: 1st sacral vertebra; SAP: superior articular process; IAP: inferior articular process; a: the crossing point of the superior and inferior articular process for 3D lumbosacral models; Line A: the shortest distance between point a and the nerve root.*

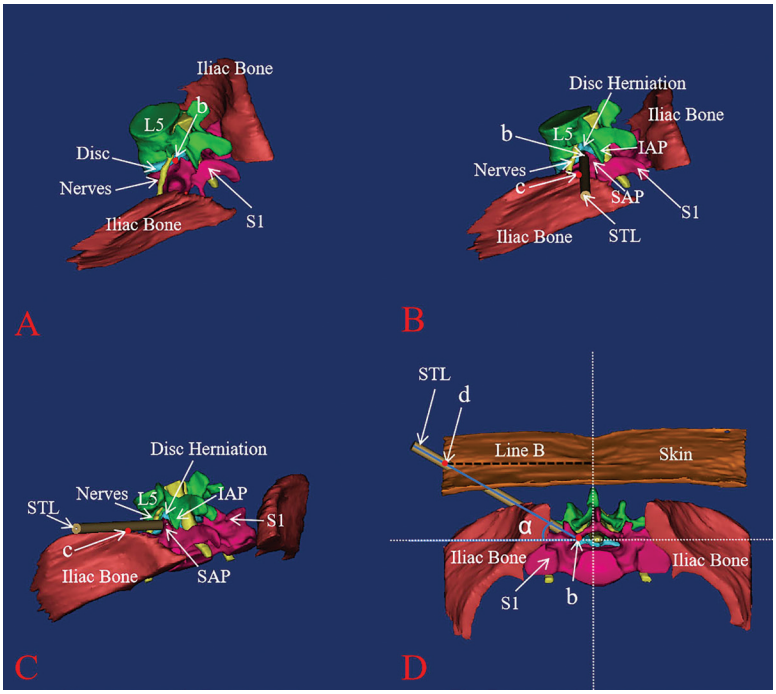

Fig. 4. *Schematic diagram of the surgical trajectory placement process in the 3D models. A, the schematic diagram of placing target point (point b); B and C, the surgical trajectory placement and its three-dimensional relationship with surrounding spinal structures; D, the measuring method of angle α and Line B. L5: 5th lumbar vertebra; S1: 1st sacral vertebra; SAP: superior articular process; IAP: inferior articular process; b: the cross-point of the medial line of the pedicle and the midline disc; c: the cross-point of the lateral line of the surgical trajectory and iliac bone; d, the cross-point of the midline surgical trajectory and skin; STL: the Standard Template Library of the surgical trajectory; α: the angle between the surgical trajectory and the coronal plane on axial view; Line B: the distance measured from the median line to point d.*

GT-3D models in Line A (P = 0.262). The mean measurements of Line A were 13.60 mm for GT-3D models and 13.47 mm for AI-3D models. Table 2 shows that ICC values between 0.999 and 0.999 are reliable for test-retests, and ICC values between 0.964 and 0.961 are reliable for multiple measurements taken by different observers.

According to the definition of Group A and Group B, out of the 100 IVF from the 50 GT-3D models, 49 (49%) were classified as Group A and 51 (51%) were classified as Group B, while from the 50 AI-3D models, 39 (39%) were classified as Group A and 61 (61%) were classified as Group B, according to the structure barriers (including the inferior articular process, transverse processes and lumbosacral nerves) of the surgical trajectory. Notably, 12 IVF (12/49) of Group A in the GT-3D models were classified as Group B in the AI-3D models, and 2 IVF (2/51) of Group B in the GT-3D models were classified as Group A in the AI-3D models. For the TF-PELD assessment of Group A (37 IVF were both classified into Group A between the GT-3D models and AI-3D models), the mean of the trajectory angle values was 40.65°and 40.33°, and the mean measurements of Line B were 89.52 mm and 90.15 mm for GT-3D and AI-3D models, respectively. There were no significant differences in the trajectory abduction angle and Line B between GT-3D and AI-3D models (P = 0.386 and P = 0.582, respectively). The trajectory abduction angle and the Line B of Group A showed high intraobserver and interobserver reliabilities (Table 3).

Discussion

3D anatomical models created from image segmentation are becoming increasingly popular for investigating virtual operative procedures, such as in spinal endoscopic surgery simulations (10,22,24). In 2016, a study developed preoperative planning software based on 3D lumbar models to identify the ideal surgical trajectory of TF-PELD (25). In another study, 3D models based on image segmentation were used to simulate the trajectory of an L5/S1 TF-PELD to guide surgical decision-making (10). The clinical feasibility of a 3D model for the surgical trajectory simulation of TF-PELD has been demonstrated (10,13), but there remains room for

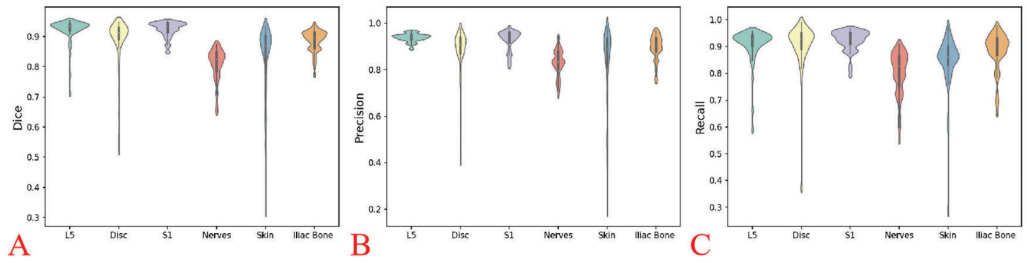

Fig. 5. *Artificial intelligence-based automated MR image segmentation achieved high mean dice score (A), precision (B), and recall (C) with 6 spinal structures including L5, Disc, S1, nerves, iliac bone and skin at the L5/S1 level.*

Table 1. *Results of automated MR image segmentation performances at the L5/S1 level.*

Performances and Data Sets		Lumbosacral Structures						
		L5	Disc	S1	Nerves	Iliac Bone	Skin	Mean
Training Set	Dice	0.953	0.938	0.958	0.884	0.942	0.927	0.927
	Precision	0.957	0.926	0.959	0.879	0.942	0.930	0.924
	Recall	0.949	0.951	0.958	0.892	0.942	0.925	0.930
Validation Set	Dice	0.922	0.881	0.919	0.805	0.868	0.746	0.849
	Precision	0.936	0.900	0.926	0.833	0.901	0.727	0.865
	Recall	0.909	0.877	0.917	0.786	0.850	0.821	0.849
Test Set	Dice	0.921	0.885	0.924	0.808	0.886	0.816	0.864
	Precision	0.939	0.879	0.928	0.830	0.897	0.821	0.875
	Recall	0.906	0.907	0.923	0.800	0.883	0.845	0.866

Note.— Data are means of 5-fold cross-validation scores. L5 = 5th lumbar vertebra bone, S1 = 1st sacral vertebra, Nerves = lumbosacral nerves.

improvement. Factors such as the type of images used to construct a 3D model, the overall completeness of the 3D model, and the accuracy and time of building a 3D model should be considered simultaneously.

3D models built in previous studies were mainly reconstructed from CT images (10,13,24). It is well known that CT scan possesses radiation and poor soft-tissue contrast properties. Notably, the reconstruction accuracy of the 3D model for soft tissues such as nerves and discs may be affected due to the poor soft-tissue contrast of the CT scan. In our study, the implementation of artificial intelligence based on automated segmentation with high-spatial-resolution MR images was conducted to address these limitations (radiation and poor soft-tissue contrast properties) of 3D models generating CT images. Image segmentation in this study was studied using MR sequence 3D T2W-SPACE (3D isotropic T2-weighted TSE sampling perfection with optimized contrasts using different flip angle evolution) (21,26). With the advantages of high-resolution multiplanar reformatted images and thin slices (26,27), MR data from the 3D T2W-SPACE sequence is more effective for demonstrating associated soft tissue structures, which has the benefit of improving the high completeness of constructing a 3D lumbar model.

Previous studies on constructing a 3D lumbar model focused on vertebrae bone segmentation (24) and disc segmentation (18,20). However, the segmentations of nerves (19,28), iliac bone (13), and skin were seldom mentioned. The segmentation of vertebrae bone and disc simultaneously on MR images has successfully achieved 3D reconstruction of the lumbar intervertebral foramen (18,20), however, this alone does not reflect the distribution of nerves and cannot accurately guide surgical treatment plans. The overall model completeness has the potential to provide detailed information on 3D anatomical structures for preoperative evaluation and surgical planning. The artificial intelligence-based automated segmentation developed in this study can effectively segment lumbosacral structures (e.g., L5 vertebrae bone, S1 vertebrae bone, discs, lumbosacral nerves, iliac crest, and skin) simultaneously. In contrast to previous studies (19,20), the automated segmentation of vertebrae bones, discs, and lumbosacral nerves was successfully achieved in our study, and the automatic segmentation of the iliac crest and skin was also performed. It benefits generating an accurate model of 3D anatomical construction to assess the relationship between critical anatomical structures and surgical channels of L5/S1 TF-PELD.

Table 2. *Test-retest reliability and interobserver reliability of Line A for all 3D models.*

Intraclass Correlation Coefficient	Test-Retest Reliability	Interobserver Reliability
Ground Truth-Derived 3D Models (GT-3D)	0.999	0.961
Artificial Intelligence-Derived 3D Models (AI-3D)	0.999	0.964

Table 3. *Test-retest reliability andinterobserver reliability of angle α and Line B for Group A.*

Intraclass Correlation Coefficient	Test-Retest Reliability	Interobserver Reliability
Angle α		
Ground Truth-Derived 3D Models (GT-3D)	0.998	0.997
Artificial Intelligence-Derived 3D Models (AI-3D)	0.999	0.998
Line B		
Ground Truth-Derived 3D Models (GT-3D)	0.999	0.999
Artificial Intelligence-Derived 3D Models (AI-3D)	0.999	0.999

The accuracy and time of building a 3D model cannot be ignored. Automated segmentation and 3D reconstruction of lumbosacral structures take only a few seconds to complete by following our method. The results showed high performance of automated segmentation. We achieved automated segmentation of the L5 vertebrae bone, S1 vertebrae bone, and disc on MR images with Dice scores of 0.921, 0.924, and 0.885, respectively, higher than those reported by Pang et al (14) (Dice scores of 0.896, 0.892, and 0.877 for the L5 vertebrae bone, S1 vertebrae bone, and disc, respectively).

Apart from the robust accuracy performances of automated segmentation, the comparison results of the shortest distance between point a and the nerve root of AI-3D models and GT-3D models, as well as Line A ($P = 0.262$), further verified the validity of the model built in this study. Previous studies proved that the relationship between the superior articular process and neural tissue is important in the surgical trajectory simulation of TF-PELD (28,29). The measured parameter used in our study was different from those in previous studies (28,29) but all of them represent the relationship between the superior articular process and neural tissue in the 3D model. The comparison of Line A between AI-3D and GT-3D models further revealed that the former generated by automated

segmentation and the latter by manual segmentation was similar.

L5/S1 TF-PELD is a demanding procedure due to the complexity of the lumbosacral anatomy. Ideally, studies of surgical trajectory will need to consider and account for the possibility of bony structure obstruction and avoid lumbosacral nerve injury (24). As a result, three angles, including coronal, sagittal, and horizontal plane, and the selection of skin entry point for the trajectory are assessed before L5/S1 TF-PELD (30). The angle between the axial projection of trajectory and the coronal line is recommended as 30-40°on the axial view (30), and the distance from the entry point to the midline of the spinous process is 120-160 mm for L5/S1 TF-PELD (31,32). However, these measured parameters of the trajectory are provided as a range, and the final surgical planning is determined by patient-specific conditions (body size, sex, and 3D anatomic features) and the surgeon's experience. In the analysis of our study, the trajectory measurement results differed for different Group A cases. The mean of the trajectory angle values in our study was 40.65°and 40.33°for GT-3D and AI-3D models, respectively, similar to a previous study (30). Interestingly, the mean measurements of Line B in our study were 89.52 mm and 90.15 mm for GT-3D and AI-3D models, respectively, both less than 120 mm, as recommended in 2 previous studies (31,32). The difference in Line B could be explained by the measured data from 3D models. This implies that our method can offer more accurate surgical trajectory measurements. Moreover, the comparison results of 3D trajectory measurements, including the trajectory angle values in axial view and the entry point distance, Line B (P = 0.386 and P = 0.582, respectively) in Group A, further demonstrated that the AI-3D model generated by automated segmentation may be the new method to help surgeons select the best surgical plan.

Our study has some limitations. First, vessel segmentation was not involved in automated magnetic resonance image segmentation in our method. Aside from nerve roots, there are vascular distributions in the extraforaminal and intraforaminal areas (33,34). Vessel segmentation should be explored in future studies. Moreover, MR imaging has a longer scanning time and higher economic cost but offers superior soft-tissue contrast in comparison with CT scanning. Finally, the sample size was small, and the findings need to be confirmed in a prospective study with a large sample size.

Conclusions

The artificial intelligence-based automated magnetic resonance image segmentation method developed in our study could effectively segment lumbosacral structures (e.g., L5 vertebrae bone, S1 vertebrae bone, disc, lumbosacral nerve, iliac bone, and skin) simultaneously on MR images. As with the manual segmentation method, a 3D lumbosacral reconstruction based on automated MR image segmentation can be a new method for selecting PELD approaches in different cases by simulating the surgical trajectory.

Acknowledgements:

Zhaoyin Zhu, Enqing Liu, and Zhihai Su contributed equally to this work and should be considered as co-first authors. Shumao Pang, Qingchu Li, and Jin Zhou are Corresponding Authors. We gratefully acknowledge the support of KetengEdit (www.Ketengedit.com), who provide a language editing service for this research.

Author Contributions

Zhaoyin Zhu, Enqing Liu, and Zhihai Su contributed equally to this work.

The manuscript submitted does not contain information about medical device(s)/drug(s). There are no relevant financial activities outside the submitted work.

Zhaoyin Zhu: Conceptualized and designed the study, acquired, analyzed, and interpreted the data, drafted and proofread the manuscript.

Enqing Liu: Conceptualized and designed the study, acquired, analyzed, and interpreted the data, drafted and proofread the manuscript.

Zhihai Su: Conceptualized and designed the study, acquired, analyzed, and interpreted the data, drafted and proofread the manuscript.

Weijian Chen: Conceptualized and designed the study, analyzed and interpreted the data, drafted and proofread the manuscript.

Zheng Liu: Conceptualized and designed the study.

Tao Chen: Acquired, analyzed, and interpreted the data.

Hai Lu: Conceptualized and designed the study.

Jin Zhou: Drafted and proofread the manuscript and gave final approval of the manuscript.

Qingchu Li: Drafted and proofread the manuscript and gave final approval of the manuscript.

Shumao Pang: Drafted and proofread the manuscript and gave final approval of the manuscript.

Funding

This study was supported by Zhuhai City Innovation and Innovation Team Project, Guangdong Province, China (ZH0406190031PWC), Zhuhai City Industry-University-Research Cooperation Project, Guangdong Province, China (ZH22017002210017PWC), Joint Funding Scheme 2022 for Scientific Research Projects (FDCT-GDST Projects) by the Science and Technology Development Fund of Macau and the Department of Science and Technology of Guangdong Province (2022A0505020019), National Natural Sciences Foundation of China (No. 62371146, 3220946, 12126603, & 2023K0604 the R&D project of Pazhou Lab (Huangpu)), and the Science and Technology Projects of Guangzhou (No. 2023C-TS25).

References

1. Lv Z, Jin L, Wang K, et al. Comparison of effects of PELD and fenestration in the treatment of geriatric lumbar lateral recess stenosis. *Clin Interven Aging* 2019; 14:2187-2194.
2. Ruetten S, Komp M, Merk H, Godolias G. Surgical treatment for lumbar lateral recess stenosis with the full-endoscopic interlaminar approach versus conventional microsurgical technique: A prospective, randomized, controlled study. *J Neurosurg Spine* 2009; 10(5):476-485.
3. Ge R, Liu Z, Huang W. Percutaneous transforaminal endoscopic discectomy is a safer approach for lumbar disc herniation. *Am Jo Transl Res* 2022; 14(9):6359-6367.
4. Huang Y, Yin J, Sun Z, et al. Percutaneous endoscopic lumbar discectomy for LDH via a transforaminal approach versus an interlaminar approach: A meta-analysis. *Orthopade* 2020; 49(4): 338-349.
5. Chen P, Hu Y, Li Z. Percutaneous endoscopic transforaminal discectomy precedes interlaminar discectomy in the efficacy and safety for lumbar disc herniation. *Biosci Rep* 2019; 39(2):BSR20181866.
6. Wu X, Fan G, Guan X, et al. Percutaneous endoscopic lumbar discectomy for far-migrated disc herniation through two working channels. *Pain Physician* 2016; 19:E675-680.
7. Chen C, Sun X, Liu J, et al. Targeted fully endoscopic visualized laminar trepanning approach under local anaesthesia for resection of highly migrated lumbar disc herniation. *Int Orthop* 2022; 46:1627-1636.
8. Patel PD, Canseco JA, Houlihan N, Gabay A, Grasso G, Vaccaro AR. Overview of minimally invasive spine surgery. *World Neurosurg* 2020; 142:43-56.
9. Lee JU, Park KJ, Kim KH, Choi MK, Lee YH, Kim DH. What is the ideal entry point for transforaminal endoscopic lumbar discectomy? *J Korean Neurosurg Soc* 2020; 63(5):614-622.
10. Jiang Y, Wang R, Chen C. Preoperative simulation of the trajectory for L5/S1 percutaneous endoscopic transforaminal discectomy: A novel approach for decision-making. *World Neurosurg* 2021; 145:77-82.
11. Yang JS, Liu KX, Kadimcherla P, et al. Can the novel lumbolliac triangle technique based on biplane oblique fluoroscopy facilitate transforaminal percutaneous endoscopic lumbar discectomy for patients with L5-S1 disc herniation combined with high iliac crest? Case-control study of 100 patients. *Pain Physician* 2020; 23(3):305-314.
12. Fan G, Liu H, Wu Z, et al. Deep learning-based automatic segmentation of lumbosacral nerves on CT for spinal intervention: A translational study. *AJNR Am J Neuroradiol* 2019; 40(6):1074-1081.
13. Fan G, Liu H, Wang D, et al. Deep learning-based lumbosacral reconstruction for difficulty prediction of percutaneous endoscopic transforaminal discectomy at L5/S1 level: A retrospective cohort study. *Int J Surg* 2020; 82:162-169.
14. Pang S, Pang C, Zhao L, et al. SpineParseNet: Spine parsing for volumetric MR image by a two-stage segmentation framework with semantic image representation. *IEEE Trans Med Imaging* 2021; 40(1):262-273.
15. Pang S, Pang C, Su Z, et al. DGMSNet: Spine segmentation for MR image by a detection-guided mixed-supervised segmentation network. *Med Image Anal* 2022; 75:102261.
16. Dourthe B, Shaikh N, Fels S, et al. Automated segmentation of spinal muscles from upright open MRI using a multi-scale pyramid 2D convolutional neural network. *Spine (Phila Pa 1976)* 2022; 47(16):1179-1186.
17. Li X, Dou Q, Chen H, et al. 3D multi-scale FCN with random modality voxel dropout learning for intervertebral disc localization and segmentation from multi-modality *MR images. Med Image Anal* 2018; 45:41-54.
18. Chen T, Su ZH, Liu Z, et al. Automated magnetic resonance image segmentation of spinal structures at the L4-5 Level with deep learning: 3D reconstruction of lumbar intervertebral roramen. *Orthop Surgery* 2022; 14(9):2256-2264.
19. Su Z, Liu Z, Wang M, et al. Three-dimensional reconstruction of Kambin's triangle based on automated magnetic resonance image segmentation. *J Orthop Res* 2022; 40(12):2914-2923.
20. Liu Z, Su Z, Wang M, et al. Computerized characterization of spinal structures on MRI and clinical significance of 3D reconstruction of lumbosacral intervertebral roramen. *Pain Physician* 2022; 25(1):E27-E35.
21. Sayah A, Jay AK, Toaff JS, Makariou EV, Berkowitz F. Effectiveness of a rapid lumbar spine MRI protocol using 3D T2-weighted SPACE imaging versus a standard protocol for evaluation of degenerative changes of the lumbar spine. *AJR Am J Roentgenol* 2016; 207(3):614-620.
22. Çiçek Ö, Abdulkadir A, Lienkamp SS, Brox T, Ronneberger O. 3D U-Net: Learning dense volumetric segmentation from sparse annotation, *International conference on medical image computing and computer-assisted intervention*. Springer, 2016, pp 424-432.
23. Landis JR, Koch GG. The measurement of observer agreement for categorical data. *Biometrics* 1977; 33(1):159-174.
24. Huang X, Zhu B, Liu X. Quantitative 3D trajectory measurement for percutaneous endoscopic lumbar discectomy. *Pain Physician* 2018; 21:E355-E365.
25. Chen X, Cheng J, Gu X, Sun Y, Politis C.

Development of preoperative planning software for transforaminal endoscopic surgery and the guidance for clinical applications. *Int J Comput Assist Radiol Surg* 2016; 11(4):613-620.

26. Sung J, Jee WH, Jung JY, et al. Diagnosis of nerve root compromise of the lumbar spine: Evaluation of the performance of three-dimensional Isotropic T2-weighted turbo spin-echo SPACE sequence at 3T. *Korean J Radiol* 2017; 18(1):249-259.
27. Wang J, Wu Y, Yao Z, Yang Z. Assessment of pituitary micro-lesions using 3D sampling perfection with application-optimized contrasts using different flip-angle evolutions. *Neuroradiology* 2014; 56(12):1047-1053.
28. Yamada K, Nagahama K, Abe Y, Hyugaji Y, Takahata M, Iwasaki N. Morphological analysis of Kambin's triangle using 3D CT/MRI fusion imaging of lumbar nerve root created automatically with artificial intelligence. *Eur Spine J* 2021; 30(8):2191-2199.
29. Hirayama J, Hashimoto M, Sakamoto T. Clinical outcomes based on preoperative Kambin's triangular working zone measurements on 3D CT/MR fusion imaging to determine optimal approaches to transforaminal endoscopic lumbar diskectomy. *J Neurol Surg A Cent Eur Neurosurg* 2020; 81(4):302-309.
30. Fan G, Wang C, Gu X, Zhang H, He S. Trajectory planning and guided punctures with isocentric navigation in posterolateral endoscopic lumbar discectomy. *World Neurosurg* 2017; 103:899-905.e4.
31. Guan X, Gu X, Zhang L, et al. Morphometric analysis of the working zone for posterolateral endoscopic lumbar discectomy based on magnetic resonance neurography. *J Spinal Disord Tech* 2015; 28(2):E78-E84.
32. Hoogland T, Schubert M, Miklitz B, Ramirez A. Transforaminal posterolateral endoscopic discectomy with or without the combination of a low-dose chymopapain: A prospective randomized study in 280 consecutive cases. *Spine (Phila Pa 1976)* 2006; 31(24):E890-E897.
33. Zhao Q, Zhong E, Shi B, Ding Z, Jin D, Li Q. Clinical anatomy and possible clinical significance of the postcentral branches of spinal arteries in the L1-L5 levels. *Clin Spine Surgery* 2020; 33(8):328-332.
34. Su Z, Wang M, Zhao Q, et al. Clinical anatomy and possible clinical significance of the intervertebral vein in the lumbar intervertebral foramina. *Pain Physician* 2019; 22(3):E225-E232.